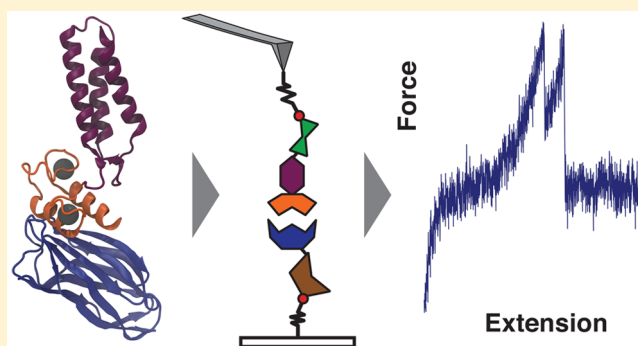


Mechanical Stability of a High-Affinity Toxin Anchor from the Pathogen *Clostridium perfringens*

Lukas F. Milles,[†] Edward A. Bayer,[‡] Michael A. Nash,^{§,⊥} and Hermann E. Gaub^{*,†,‡}[†]Lehrstuhl für Angewandte Physik and Center for Nanoscience, Ludwig-Maximilians-University, Amalienstr. 54, 80799 Munich, Germany[‡]Department of Biomolecular Sciences, The Weizmann Institute of Science, Rehovot 76100, Israel[§]Department of Chemistry, University of Basel, Klingelbergstr. 80, 4056 Basel, Switzerland[⊥]Department of Biosystems Science and Engineering, Eidgenössische Technische Hochschule Zürich (ETH-Zürich), Mattenstr. 26, 4058 Basel, Switzerland

ABSTRACT: The opportunistic pathogen *Clostridium perfringens* assembles its toxins and carbohydrate-active enzymes by the high-affinity cohesin-dockerin (Coh-Doc) interaction. Coh–Doc interactions characterized previously have shown considerable resilience toward mechanical stress. Here, we aimed to determine the mechanics of this interaction from *C. perfringens* in the context of a pathogen. Using atomic force microscopy based single-molecule force spectroscopy (AFM-SMFS) we probed the mechanical properties of the interaction of a dockerin from the μ -toxin with the GH84C X82 cohesin domain of *C. perfringens*. Most probable complex rupture forces were found to be approximately 60 pN and an estimate of the binding potential width was performed. The dockerin was expressed with its adjacent FIVAR (found in various architectures) domain, whose mechanostability we determined to be very similar to the complex. Additionally, fast refolding of this domain was observed. The Coh-Doc interaction from *C. perfringens* is the mechanically weakest observed to date. Our results establish the relevant force range of toxin assembly mechanics in pathogenic *Clostridia*.



INTRODUCTION

Clostridium perfringens is an anaerobic, Gram-positive, rod-shaped bacterium found within the human gut that commonly causes food-borne illnesses, gastrointestinal disease, and tissue necrosis.¹ The bacterium secretes an arsenal of toxins, glycoside hydrolases (GHs), and carbohydrate-binding modules (CBMs) thought to degrade extracellular matrix polysaccharides, as well as gastric mucins (gut-lining proteins). It was previously found that bimolecular complexes between the glycoside hydrolase domains (e.g., sialidase) and the so-called μ -toxin domain are held together using high-affinity receptor–ligand pairs that structurally resemble the cohesin-dockerin (Coh-Doc) complexes found among multienzyme complexes involved in biomass conversion (i.e., cellulosomes).² The dockerin shows the characteristic EF-hand-like dual calcium-binding loops. FIVAR (found in various architectures) is a motif found in other pathogenic bacteria, e.g., *Staphylococci*, and consists of a 9-kDa three-helix bundle. A pair of GH84C X82 cohesin (Coh, shown in Figure 1 in blue) and FIVAR-dockerin (FIVAR-Doc, shown in Figure 1 in purple and orange, respectively) complexes from this family 84 GH was previously identified and found to have high binding affinities ($K_D < 1$ nM).^{3–5}

With the goal of improving our understanding of the mechanical properties of toxin-forming complexes derived from

pathogenic clostridia, we report here on the binding strength of one such complex, a native FIVAR-Doc:Coh complex from *C. perfringens* measured at the single-molecule level. We use an atomic force microscope (AFM) operated in single-molecule force spectroscopy mode (SMFS) to understand how these protein modules unfold and dissociate under applied mechanical stress.^{6,7} Furthermore, we determine the force loading rate dependence of the rupture force and estimate the distance to the transition state and the natural off-rate at zero force.

We find that under mechanical perturbation, the FIVAR domain usually unfolds prior to cohesin-dockerin rupture. Compared to several other cohesin-dockerin systems, the FIVAR-Doc:Coh complex shows weaker rupture events of approximately 60 pN at loading rates of 10^3 – 10^4 pN/s.¹ To put this in context, the type I interaction of dockerin from Cel48S and the second cohesin from CipA from *Clostridium thermocellum* ruptures in the range of 120 pN.^{8,9} The type III

Special Issue: Klaus Schulten Memorial Issue

Received: September 22, 2016

Revised: November 9, 2016

Published: November 10, 2016

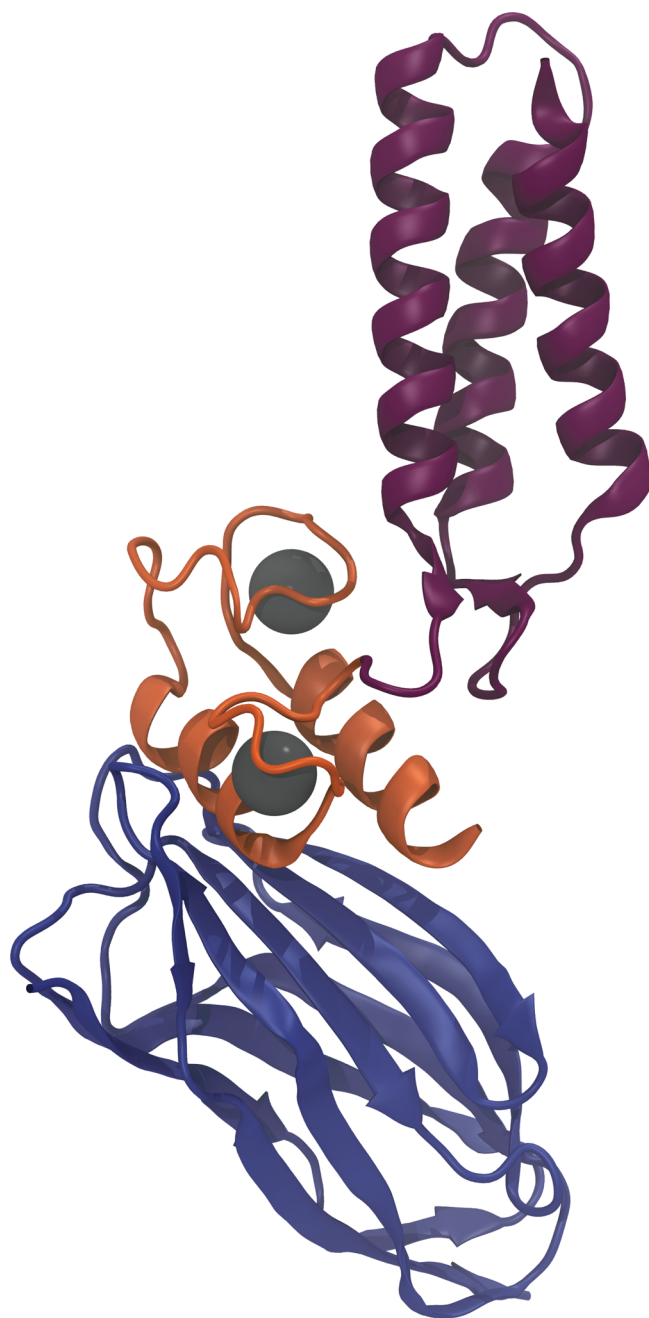


Figure 1. Crystal structure of the FIVAR-Doc:Coh complex (PDB accession: 2OZN, rendering in VMD³⁶). The three-helix bundle of FIVAR (purple) is fused to the Doc domain (orange) with its two calcium (gray spheres) binding loops and binds the immunoglobulin-like fold of the Coh (blue).

cohesin-dockerin interaction of CttA Xmodule-dockerin and CohesinE (both from *Ruminococcus flavefaciens*) withstands even higher forces of more than 600 pN at similar pulling velocities.¹⁰ The *C. perfringens* cohesin-dockerin interaction is therefore the weakest measured to date. Significantly, our results identify FIVAR as a potentially useful candidate domain for incorporation into engineered polyprotein constructs for single-molecule force spectroscopy studies as a refolding fingerprint domain.¹¹ The *C. perfringens* Coh-Doc is an ideal protein receptor–ligand system when low complex rupture forces (~60 pN) yet high thermodynamic affinities are desired.

METHODS

Gene Construction and Protein Expression. The carbohydrate binding module gene is part of CipA from *C. thermocellum*. The *Dictyostelium discoideum* fourth filamin domain (ddFLN4) gene was synthesized codon-optimized for expression in *Escherichia coli* as a linear DNA fragment (GeneArt – ThermoFisher Scientific, Regensburg, Germany). The Coh and FIVAR-Doc genes from *C. perfringens* were synthesized codon optimized for *E. coli* (Centic Biotech, Heidelberg, Germany). All plasmids were cloned using the Gibson assembly strategy¹² (New England Biolabs, MA, USA) into pET28a Vectors. The C63S mutation in the CBM had been introduced previously with blunt end ligation cloning using T4 Ligase. All final open reading frames were checked by DNA sequencing (Eurofins Genomics, Ebersberg, Germany).

Protein Expression and Purification. Proteins were expressed with the ybbr-tag.¹³ Coh-CBM(C63S)-ybbr and ybbr-ddFLN4-FIVAR-Doc fusion proteins were expressed in *E. coli* NiCo21(DE3) (New England Biolabs, MA, USA). Precultures of 5 mL in LB medium, grown overnight at 37 °C, were inoculated in ZYM-5052 autoinduction media containing kanamycin and grown for 6 h at 37 °C and then 24 h at 25 °C.¹⁴ Bacteria were spun down, and stored frozen at –80 °C. The pellet was resuspended and cells were lysed through sonication followed by centrifugation at 18 000 g for 1 h. The supernatant was applied to a Ni-NTA column (GE Healthcare, MA, USA) for HIS-Tag purification and washed extensively. The protein was eluted with 200 mM imidazole. Protein containing fractions were concentrated over regenerated cellulose filters (Amicon, Merck, Darmstadt, Germany), exchanged into measurement buffer (TBS-Ca: 25 mM Tris, 72 mM NaCl, 1 mM CaCl₂) by polyacrylamide columns (Zeba, Thermo Scientific, MA, USA), and frozen with 25% (v/v) glycerol in liquid nitrogen to be stored at –80 °C until used in experiments. Protein concentrations were measured with spectrophotometry to be 12 mg/mL (434 μM) for ybbr-ddFLN4-FIVAR-Doc and 31 mg/mL (787 μM) for Coh-CBM-ybbr (on a NanoDrop 1000, Thermo Scientific, DE, USA).

AFM Sample Preparation. A complete AFM-SMFS protocol has been published previously.¹⁵ AFM Cantilevers (Biolever Mini, Olympus, Tokyo, Japan) and cover glass surfaces are modified identically. In brief, after UV-Ozone cleaning, surfaces were incubated in (3-aminopropyl)-dimethyl-ethoxysilane (APDMES, abcr, Karlsruhe, Germany) baked at 80 °C for 1 h and stored overnight under argon. Both surfaces were covered with 5 kDa heterobifunctional Succinimide-PEG-Maleimide (Rapp Polymere, Tübingen, Germany) dissolved in sodium borate buffer (pH 8.5) for 30 min. After rinsing with ultrapure water, 20 mM Coenzyme A in a 50 mM sodium phosphate pH 7.2, 50 mM NaCl, 10 mM EDTA buffer was applied for 1 h. The protein samples were exchanged into TBS-Ca supplemented with 10 mM MgCl₂. After rinsing in water again, the cantilevers were incubated with 40 μM ybbr-ddFLN4-FIVAR-Doc and 28 μM Sfp phosphopantetheinyl transferase (SFP) for 2 h. The glass surfaces were incubated with 1–10 μM Coh-CBM-ybbr and 14 μM SFP for 30 min. Both samples were rinsed extensively with at least 30 mL TBS-Ca before measurement.

AFM-SMFS. AFM-SMFS data was acquired on a custom-built AFM operated in closed loop by a MFP3D controller (Asylum Research, Santa Barbara, CA, USA) programmed in Igor Pro 6 (Wavemetrics, OR, USA). Cantilevers were briefly

brought in contact with the functionalized surface and then retracted at constant velocities of 400, 800, 1600, and 3200 nm/s. Following each curve, the glass surface was moved horizontally by 100 nm to expose an unused surface area. Typically, 80 000 curves were recorded. Cantilevers were calibrated using the equipartition theorem method with typical spring constants between 50 and 110 pN/nm.¹⁶

SMFS Data Analysis. Data analysis was carried out in Python 2.7 (Python Software Foundation).^{17–19} Raw data were transformed from photodiode and piezo voltages into physical units with the cantilever calibration and piezo sensitivity. Laser spot drift on the cantilever relative to the calibration curve was corrected via the baseline noise for all curves. The last rupture peak was detected and the subsequent 20 nm were used to set the force baseline to zero. The origin of extension was then set as the first and closest point to zero force. A correction for cantilever bending given through the forces measured was applied to the extension data points. For peak detection, data were denoised with Total Variation Denoising (TVD, denoised data not shown),^{20,21} and rupture events detected as significant drops in force. Peaks were assigned in contour length space diagrams assembled through Kernel Density Estimates with a bandwidth of 1 nm. The Worm Like Chain model (WLC)²² was used to fit relevant peaks. The loading rate was fitted as the linear slope of the last 4 nm preceding a peak. Rupture force histograms and dynamic force spectra were assembled from all curves showing the FIVAR fingerprint, which could be fitted in good agreement with the WLC model. The most probable loading rate was determined with a Kernel Density Estimate, with the bandwidth chosen by the Silverman estimator.²³ This value was used to fit the unfolding or rupture force histograms following Schulten and colleagues for each pulling velocity, yielding the most probable unfolding or rupture force.^{24,25} A final fit was performed through these most probable forces and loading rates over all pulling velocities to determine the distance to the transition state Δx_0 and natural off-rate at zero force $k_{\text{off},0}$. Errors in Figures 2e and 3d are given as the asymmetric full width at half-maximum (fwhm) of each probability distribution.

RESULTS AND DISCUSSION

To investigate the mechanical stability of the *C. perfringens* GH84C X82 cohesin and μ -toxin dockerin complex, we expressed the proteins as fusion constructs with refolding fingerprint domains of a known unfolding pattern and rupture force to facilitate screening of force curves for specific tethers. The FIVAR-Doc was expressed with the fourth filamin domain of *Dictyostelium discoideum*. This domain typically unfolds at forces around 80 pN when tethered with cantilevers of similar stiffness.²⁶ The Coh was cloned into a fusion protein with a CBM from CipA of *C. thermocellum*, with its cysteine at residue 63 mutated to a serine. This domain is known to unfold at forces around 140 pN under comparable experimental conditions. The Coh was expressed as both Coh-CBM-ybbr for C-terminal tethering and ybbr-CBM-Coh for N-terminal pulling (data not shown).

Both proteins were site specifically coupled to Coenzyme A via the ybbr tag.³ The ddFLN4-FIVAR-Doc, which is located at the C-terminus of the μ -toxin was tethered from the N-terminus, as force under physiological conditions can only be applied from this end. FIVAR-Doc was immobilized on the cantilever to probe surface bound Coh, see Figure 2a.

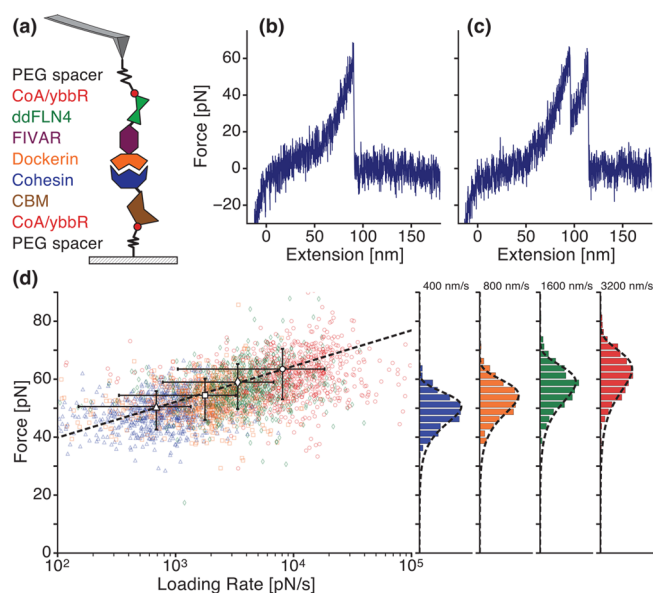


Figure 2. SMFS on the *C. perfringens* FIVAR-Doc:Coh complex. (a) Experimental setup with the ddFLN4-FIVAR-Doc immobilized on the cantilever and the Coh-CBM bound to the surface. A typical force–extension trace for a Coh-Doc complex rupture event without (b) and with (c) preceding unfolding of the FIVAR domain. (d) Dynamic force spectrum for Coh-Doc complex rupture with FIVAR unfolding as fingerprint. The respective pulling velocities were 400 nm/s (blue triangles), 800 nm/s (orange squares), 1600 nm/s (green diamonds), and 3200 nm/s (red circles). The corresponding rupture force histograms and individual distribution fits (black dashed lines) are projected onto the right axes. The fit through the most probable rupture force and force loading rate (black, dashed line through white markers) is shown on the left with error bars given as the fwhm for each distribution. The force loading rate was determined as a linear fit through the 4 nm preceding a peak.

Experimental runs were screened for specific events, yet the signature of the CBM was not observed and ddFLN4 with its characteristic unfolding intermediate²⁶ only appeared in less than 3% ($N = 3925$) of traces showing a clear single tether. The complex rupture forces peaking around 60 pN were too low to unfold any of the fingerprint domains with high probability in every trace as shown in an exemplary trace Figure 2b.

Despite this lack of a standard fingerprint, a domain unfolding event corresponding to a single contour length increment of around 28 nm was found in 83% of the total usable traces ($N = 3925$), both with FIVAR-Doc on the cantilever or the surface, see Figure 2c. The distance of this increment was measured by averaging the contour length diagrams for each curve aligned to the contour length of the complex rupture and measuring the expected contour length increment, as shown in Figure 3d.²⁷

We assigned this increment to the FIVAR domain. The expected contour length increment for FIVAR unfolding was calculated as follows: the length of unfolded FIVAR peptide chain corresponding to 79 amino acids (aspartic acid 1498 to threonine 1577) at 0.4 nm per residue minus the distance of these residues in the folded protein determined from the crystal structure (4 nm) as shown in Figure 3a. The expected contour length increment thus is 27.6 nm, which is in very good agreement with the 28 nm contour length increment given by the alignment. As the unfolding forces of the CBM and ddFLN4 fingerprints were significantly larger than the complex rupture forces, only extremely rarely a ddFLN4 unfolded prior

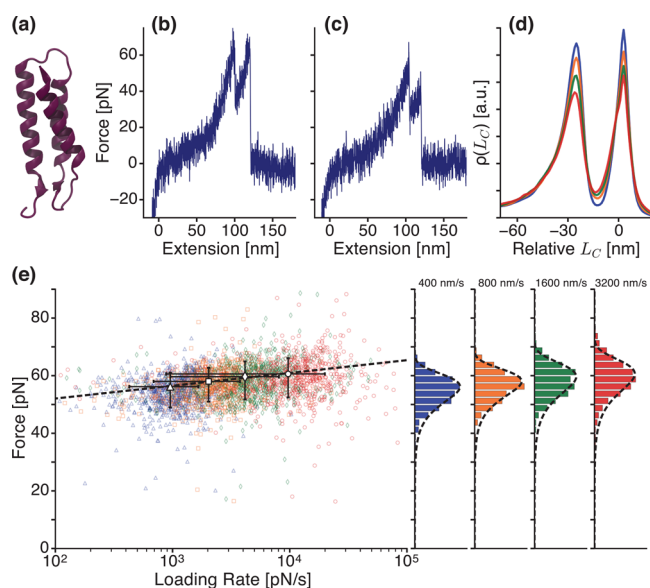


Figure 3. SMFS characterization of FIVAR unfolding events. (a) Close-up of the three-helix crystal structure of the FIVAR domain. (b) A typical force–extension trace for a Coh-Doc rupture event preceded by unfolding of the FIVAR domain. (c) The common case of a shielded unfolding event, where the complex rupture force is lower than that of FIVAR domain unfolding. (d) Relative contour length probability density functions of all traces showing FIVAR unfolding ($N = 3012$) aligned to the contour length of the complex rupture peak for each pulling velocity. The unfolded contour length is the distance between the peaks, $\Delta L_c = 28$ nm. Color coding is the same as indicated for panel (e). (e) Dynamic force spectrum for FIVAR unfolding. The respective pulling velocities were 400 nm/s (blue triangles), 800 nm/s (orange squares), 1600 nm/s (green diamonds), and 3200 nm/s (red circles). The corresponding rupture force histograms and individual distribution fits (black dashed lines) are projected onto the right axes. The fit through the most probable rupture force and force loading rate (black, dashed line through white markers) is shown on the left with error bars given as the fwhm for each distribution. The force loading rate was determined as a linear fit through the 4 nm preceding a peak.

to complex rupture. Thus, our fingerprints were not suitable to screen curves.

We therefore used the FIVAR domain unfolding event as an indicator of specific binding instead, and only included curves with the 28 nm increment in the final analysis as shown in Figure 3b and c. Some force extension curves show a shielded behavior, where the unfolding of FIVAR occurs at higher forces than the complex rupture, see Figure 3c. As FIVAR unfolding and complex rupture are stochastic processes, these shielded events are explained by the large overlap of the probability density distributions for unfolding or complex rupture, both peaking around 60 pN.

The mechanical stability of the FIVAR domain and Coh-Doc interaction were probed at constant pulling velocities of 400, 800, 1600, 3200 nm/s. The most probable unfolding force of FIVAR peaked at 56 to 60 pN, increasing with retraction velocity. Notably, FIVAR unfolded in 83% of traces, also when tethered on the cantilever. The number of FIVAR-Doc molecules on the cantilever tip is limited, yet FIVAR signatures did not cease to appear over the course of an overnight experiment. Thus, we conclude that FIVAR refolds quickly on a time scale of a pulling cycle, typically <1 s. Using a linear fit of the 4 nm preceding the unfolding event to determine the force

loading rate, we found $\Delta x_0 = 2.1 \pm 0.25$ nm and $k_{\text{off},0} = 9.7 \times 10^{-11} \pm 3.4 \times 10^{-10}$ s $^{-1}$ for FIVAR unfolding, as shown in the dynamic force spectrum in Figure 3e. For this analysis, $N = 2981$ curves were evaluated.

Finally, we determined the mechanical stability of the Coh-Doc interaction from the complex rupture peak. To ensure specific tethering we only included traces showing FIVAR unfolding. The most probable complex rupture forces ranged from 50 to 63 pN. When using a linear fit of the 4 nm preceding complex rupture to determine the loading rate, we found $\Delta x_0 = 0.77 \pm 0.055$ nm and $k_{\text{off},0} = 0.011 \pm 0.0076$ s $^{-1}$, shown in the dynamic force spectrum in Figure 2d. For this analysis, $N = 2915$ curves were evaluated. All fitted data were recorded with a single cantilever, so calibration error differences can be excluded and absolute forces compared.

Among Coh-Doc complexes investigated previously with SMFS the mechanical strength of Coh-Doc from *C. perfringens* is the lowest reported to date. It is only half of the rupture forces of 100 to 150 pN for type I Coh-Doc from *C. thermocellum*. Some type I dockerins may also display a dual binding mode that has been characterized previously through the appearance of a short unfolding event preceding final complex rupture.^{9,28} No such events were observed here, and a dual binding mode seems unlikely for this interaction, due to a lack of symmetry in the Doc. Coh-Doc stability of *C. perfringens* is almost an order of magnitude lower in force than the type III cohesin dockerin interaction, which reaches 600 pN and is stabilized by an X-module, that the system investigated here lacks. The affinity of the *C. perfringens* complex with a K_D estimated to lie below 1 nM is very similar to the affinity of the type I interaction on the order of 10 pM and comparable to type III with about 20 nM.^{29,30} The mechanics of this complex, however, are less stable, demonstrating that affinity and mechanostability are not necessarily correlated, even when comparing proteins of the same fold family with very similar motifs, such as the EF-hand-like motif calcium binding loops of dockerins.

The loading rate dependency of the rupture force of the FIVAR domain is noticeably less steep than that of the Coh-Doc complex. This can be interpreted as a “melting” rather than sudden unfolding that can be attributed to the mechanically less stable α -helical structure of the FIVAR domain. This behavior is manifested in its very low natural off-rate in the range of 1×10^{-11} s $^{-1}$, albeit this value showing a large uncertainty. Additionally, the FIVAR fingerprint unfolding and the Coh-Doc complex unbinding occur at very similar forces. Hence, a recently described selection bias effect might skew the FIVAR rupture force distribution toward lower forces.^{9,31} The strongly overlapping probability densities of FIVAR unfolding and Coh-Doc unbinding hinder a complete sampling of the FIVAR rupture forces. The strength of the pulling handle determines the upper limit of the force range accessible. Accordingly, FIVAR could withstand higher force values, yet the pulling handle is too weak to probe these. The quantitative magnitude of this bias is difficult to estimate in the constant speed protocol applied here. A worst-case estimate for comparable loading rates results in a systematic reduction of mean rupture forces by about 10–20% from their unbiased values.³¹ Under the reasonable assumption that after FIVAR unfolding the system resets to a force outside the range of probable unbinding forces the receptor–ligand distribution remains largely unaffected by this effect.

Previously investigated coiled-coil, α -helical proteins have shown lower unfolding forces. Notably, the cytoskeletal protein spectrin unfolds at 25–35 pN at similar force loading rates.³² Strikingly, the unfolding forces of FIVAR are almost twice as large. Considering that FIVAR was not investigated individually with a different pulling handle, it cannot be excluded that the Doc stabilizes the FIVAR fold. However, the reverse does not hold. Comparing traces with FIVAR unfolding and those without yielded no major change in unbinding forces of Coh-Doc. Conversely, we conclude that FIVAR does not contribute to the stability of the interaction.

FIVAR's biological role is not entirely clear. Structurally, it shows similarities to heparin binding proteins.³ More recently the FIVAR domain repeats of an extracellular matrix binding protein from *S. epidermidis* have been found to interact with surface-immobilized fibronectin.^{3,33} As force applied from the N-terminus would propagate through the FIVAR domains and unfold them mainly before the Coh-Doc complex dissociates, one could speculate that FIVAR in this setting acts as a mechanical buffer, unfolding before the complex and dissipating energy.³⁴ As FIVAR refolds very quickly when forces return to zero, it can repeat this process repeatedly, and resume its presumed binding function. The combination of reliable refolding, low unfolding forces, a constant contour length increment, and small molecular weight of only approximately 9 kDa makes FIVAR an excellent fingerprinting molecule for future studies.

CONCLUSION

We have characterized the mechanics of a cohesin-dockerin interaction from *C. perfringens* and its α -helical FIVAR domain. FIVAR unfolds at similar forces as the Coh-Doc complex of around 60 pN, and is a suitable fingerprint molecule featuring a single contour length increment, small molecular weight, comparatively low unfolding forces, and rapid refolding for use on the cantilever side. Overall, the rupture force of around 60 pN of the *C. perfringens* system establishes a force regime for pathogenic toxin assembly and extends the cohesin-dockerin toolbox. The high affinity yet moderate unbinding forces make the cohesin-dockerin interaction from *C. perfringens* a prominent candidate for designing constructs for single-molecule cut and paste surface assembly³⁵ or as a small protein pulldown tag.

AUTHOR INFORMATION

Corresponding Author

*E-mail: gaub@lmu.de; Telephone: +49 (0) 89/2180-3172.

ORCID

Hermann E. Gaub: 0000-0002-4220-6088

Notes

The authors declare no competing financial interest.

ACKNOWLEDGMENTS

This article is dedicated to the late Klaus Schulten, a brilliant colleague, mentor, and friend. We gratefully acknowledge funding from an advanced grant of the European Research Council (Cellufuel Grant 294438) and from the Deutsche Forschungsgemeinschaft SFB 863, as well as support from the GIF, the German-Israeli Foundation for Scientific Research and Development.

REFERENCES

- (1) Rood, J. I.; Cole, S. T. Molecular Genetics and Pathogenesis of *Clostridium Perfringens*. *Microbiol. Rev.* **1991**, *55*, 621–648.
- (2) Bayer, E. A.; Belaich, J.-P.; Shoham, Y.; Lamed, R. The Cellulosomes: Multienzyme Machines for Degradation of Plant Cell Wall Polysaccharides. *Annu. Rev. Microbiol.* **2004**, *58*, 521–554.
- (3) Chitayat, S.; Adams, J. J.; Furness, H. S. T.; Bayer, E. A.; Smith, S. P. The Solution Structure of the C-Terminal Modular Pair from *Clostridium Perfringens* μ -Toxin Reveals a Noncellulosomal Dockerin Module. *J. Mol. Biol.* **2008**, *381*, 1202–1212.
- (4) Adams, J. J.; Gregg, K.; Bayer, E. A.; Boraston, A. B.; Smith, S. P. Structural Basis of *Clostridium Perfringens* Toxin Complex Formation. *Proc. Natl. Acad. Sci. U. S. A.* **2008**, *105*, 12194–12199.
- (5) Chitayat, S.; Gregg, K.; Adams, J. J.; Ficko-Blean, E.; Bayer, E. A.; Boraston, A. B.; Smith, S. P. Three-Dimensional Structure of a Putative Non-Cellulosomal Cohesin Module from a *Clostridium Perfringens* Family 84 Glycoside Hydrolase. *J. Mol. Biol.* **2008**, *375*, 20–28.
- (6) Churnside, A.; Sullan, R.; Nguyen, D.; Case, S.; Bull, M.; King, G.; Perkins, T. Routine and Timely Sub-picoNewton Force Stability and Precision for Biological Applications of Atomic Force Microscopy. *Nano Lett.* **2012**, *12*, 3557–3561.
- (7) Rief, M.; Gautel, M.; Oesterhelt, F.; Fernandez, J. M.; Gaub, H. E. Reversible Unfolding of Individual Titin Immunoglobulin Domains by AFM. *Science* **1997**, *276*, 1109–1112.
- (8) Stahl, S. W.; Nash, M. A.; Fried, D. B.; Slutzki, M.; Barak, Y.; Bayer, E. A.; Gaub, H. E. Single-Molecule Dissection of the High-Affinity Cohesin-Dockerin Complex. *Proc. Natl. Acad. Sci. U. S. A.* **2012**, *109*, 20431.
- (9) Jobst, M. A.; Milles, L. F.; Schoeler, C.; Ott, W.; Fried, D. B.; Bayer, E. A.; Gaub, H. E.; Nash, M. A. Resolving Dual Binding Conformations of Cellulosome Cohesin-Dockerin Complexes Using Single-Molecule Force Spectroscopy. *eLife* **2015**, *4*, 1–19.
- (10) Schoeler, C.; Malinowska, K. H.; Bernardi, R. C.; Milles, L. F.; Jobst, M. A.; Durner, E.; Ott, W.; Fried, D. B.; Bayer, E. A.; Schulten, K.; et al. Ultrastable Cellulosome-Adhesion Complex Tightens under Load. *Nat. Commun.* **2014**, *5*, 5635.
- (11) Ott, W.; Jobst, M. A.; Schoeler, C.; Gaub, H. E.; Nash, M. A. Single-Molecule Force Spectroscopy on Polypeptides and Receptor-ligand Complexes: The Current Toolbox. *J. Struct. Biol.* **2016**, *S1047*.
- (12) Gibson, D. G.; Young, L.; Chuang, R.-Y.; Venter, J. C.; Hutchison, C. A.; Smith, H. O. Enzymatic Assembly of DNA Molecules up to Several Hundred Kilobases. *Nat. Methods* **2009**, *6*, 343–345.
- (13) Yin, J.; Straight, P. D.; McLoughlin, S. M.; Zhou, Z.; Lin, A. J.; Golan, D. E.; Kelleher, N. L.; Kolter, R.; Walsh, C. T. Genetically Encoded Short Peptide Tag for Versatile Protein Labeling by Sfp Phosphopantetheinyl Transferase. *Proc. Natl. Acad. Sci. U. S. A.* **2005**, *102*, 15815–15820.
- (14) Studier, F. W. Protein Production by Auto-Induction in High-Density Shaking Cultures. *Protein Expression Purif.* **2005**, *41*, 207–234.
- (15) Jobst, M. A.; Schoeler, C.; Malinowska, K.; Nash, M. A. Investigating Receptor-Ligand Systems of the Cellulosome with AFM-Based Single-Molecule Force Spectroscopy. *J. Visualized Exp.* **2013**, 1–10.
- (16) Hutter, J. L.; Bechhoefer, J. Calibration of Atomic-Force Microscope Tips. *Rev. Sci. Instrum.* **1993**, *64*, 1868–1873.
- (17) Hunter, J. D. Matplotlib: A 2D Graphics Environment. *Comput. Sci. Eng.* **2007**, *9*, 90–95.
- (18) Pedregosa, F.; Varoquaux, G.; Gramfort, A.; Michel, V.; Thirion, B.; Grisel, O.; Blondel, M.; Prettenhofer, P.; Weiss, R.; Dubourg, V.; et al. Scikit-Learn: Machine Learning in Python. *J. Mach. Learn. Res.* **2011**, *12*, 2825–2830.
- (19) van der Walt, S.; Colbert, S. C.; Varoquaux, G. The NumPy Array: A Structure for Efficient Numerical Computation. *Comput. Sci. Eng.* **2011**, *13*, 22–30.
- (20) Condat, L. A Direct Algorithm for 1-D Total Variation Denoising. *IEEE Signal Process. Lett.* **2013**, *20*, 1054–1057.
- (21) Rudin, L.; Osher, S.; Fatemi, E. Nonlinear Total Variation Based Noise Removal Algorithms. *Phys. D* **1992**, *60*, 259–268.

- (22) Bustamante, C.; Marko, J. F.; Siggia, E. D.; Smith, S. Entropic Elasticity of Lambda-Phage DNA. *Science* **1994**, *265*, 1599–1600.
- (23) Silverman, B. Density Estimation for Statistics and Data Analysis. *Monographs on Statistics and Applied Probability* **1986**, *37*, 176.
- (24) Izrailev, S.; Stepaniants, S.; Balsera, M.; Oono, Y.; Schulten, K. Molecular Dynamics Study of Unbinding of the Avidin-Biotin Complex. *Biophys. J.* **1997**, *72*, 1568–1581.
- (25) Evans, E.; Ritchie, K. Dynamic Strength of Molecular Adhesion Bonds. *Biophys. J.* **1997**, *72*, 1541–1555.
- (26) Schwaiger, I.; Kardinal, A.; Schleicher, M.; Noegel, A. A.; Rief, M. A Mechanical Unfolding Intermediate in an Actin-Crosslinking Protein. *Nat. Struct. Mol. Biol.* **2004**, *11*, 81–85.
- (27) Puchner, E. M.; Franzen, G.; Gautel, M.; Gaub, H. E. Comparing Proteins by Their Unfolding Pattern. *Biophys. J.* **2008**, *95*, 426–434.
- (28) Carvalho, A. L.; Dias, F. M. V.; Nagy, T.; Prates, J. A. M.; Proctor, M. R.; Smith, N.; Bayer, E. A.; Davies, G. J.; Ferreira, L. M. A.; Romão, M. J.; et al. Evidence for a Dual Binding Mode of Dockerin Modules to Cohesins. *Proc. Natl. Acad. Sci. U. S. A.* **2007**, *104*, 3089–3094.
- (29) Salama-Alber, O.; Jobby, M. K.; Chitayat, S.; Smith, S. P.; White, B. A.; Shimon, L. J. W.; Lamed, R.; Frolow, F.; Bayer, E. A. Atypical Cohesin-Dockerin Complex Responsible for Cell Surface Attachment of Cellulosomal Components: Binding Fidelity, Promiscuity, and Structural Buttresses. *J. Biol. Chem.* **2013**, *288*, 16827–16838.
- (30) Mechaly, A.; Fierobe, H. P.; Belaich, A.; Belaich, J. P.; Lamed, R.; Shoham, Y.; Bayer, E. A. Cohesin-Dockerin Interaction in Cellulosome Assembly: A Single Hydroxyl Group of a Dockerin Domain Distinguishes between Nonrecognition and High Affinity Recognition. *J. Biol. Chem.* **2001**, *276*, 9883–9888.
- (31) Schoeler, C.; Verdorfer, T.; Gaub, H. E.; Nash, M. A. Biasing Effects of Receptor-Ligand Complexes on Protein-Unfolding Statistics. *Phys. Rev. E: Stat. Phys., Plasmas, Fluids, Relat. Interdiscip. Top.* **2016**, *94*, 42412.
- (32) Rief, M.; Pascual, J.; Saraste, M.; Gaub, H. E. Single Molecule Force Spectroscopy of Spectrin Repeats: Low Unfolding Forces in Helix Bundles. *J. Mol. Biol.* **1999**, *286*, 553–561.
- (33) Christner, M.; Franke, G. C.; Schommer, N. N.; Wendt, U.; Wegert, K.; Pehle, P.; Kroll, G.; Schulze, C.; Buck, F.; Mack, D.; et al. The Giant Extracellular Matrix-Binding Protein of *Staphylococcus Epidermidis* Mediates Biofilm Accumulation and Attachment to Fibronectin. *Mol. Microbiol.* **2010**, *75*, 187–207.
- (34) Echelman, D. J.; Alegre-Cebollada, J.; Badilla, C. L.; Chang, C.; Ton-That, H.; Fernández, J. M. CnaA Domains in Bacterial Pili Are Efficient Dissipaters of Large Mechanical Shocks. *Proc. Natl. Acad. Sci. U. S. A.* **2016**, *113*, 2490–2495.
- (35) Pippig, D. A.; Baumann, F.; Strackharn, M.; Aschenbrenner, D.; Gaub, H. E. Protein–DNA Chimeras for Nano Assembly. *ACS Nano* **2014**, *8*, 6551–6555.
- (36) Humphrey, W.; Dalke, A.; Schulten, K. VMD: Visual Molecular Dynamics. *J. Mol. Graphics* **1996**, *14*, 33–38.